

On Sparse Identification of Complex Dynamical Systems: A Study on Discovering Influential Reactions in Chemical Reaction Networks

Farshad Harirchi^a, Doohyun Kim^b, Omar Khalil^a, Sijia Liu^a, Paolo Elvati^b,
Mayank Baranwal^a, Alfred Hero^{a,*}, Angela Violi^{b,c,*}

^a*Department of Electrical Engineering and Computer Science, University of Michigan, Ann Arbor, MI 48109-2125, USA*

^b*Department of Mechanical Engineering, University of Michigan, Ann Arbor, MI 48109-2125, USA*

^c*Departments of Chemical Engineering, Biomedical Engineering, Macromolecular Science and Engineering, Biophysics Program, University of Michigan, Ann Arbor, MI 48109-2125, USA*

Abstract

A wide variety of real life complex networks are prohibitively large for modeling, analysis and control. Understanding the structure and dynamics of such networks entails creating a smaller representative network that preserves its relevant topological and dynamical properties. While modern machine learning methods have enabled identification of governing laws for complex dynamical systems, their inability to produce white-box models with sufficient physical interpretation renders such methods undesirable to domain experts. In this paper, we introduce a hybrid black-box, white-box approach for the sparse identification of the governing laws for complex, highly coupled dynamical systems with particular emphasis on finding the influential

*Corresponding authors:

Email addresses: hero@eecs.umich.edu (Alfred Hero), avioli@umich.edu (Angela Violi)

reactions in chemical reaction networks for combustion applications, using a data-driven sparse-learning technique. The proposed approach identifies a set of influential reactions using species concentrations and reaction rates, with minimal computational cost without requiring additional data or simulations. The new approach is applied to analyze the combustion chemistry of H_2 and C_3H_8 in a constant-volume homogeneous reactor. The influential reactions determined by the sparse-learning method are consistent with the current kinetics knowledge of chemical mechanisms. Additionally, we show that a reduced version of the parent mechanism can be generated as a combination of the significantly reduced influential reactions identified at different times and conditions and that for both H_2 and C_3H_8 fuel, the reduced mechanisms perform closely to the parent mechanisms as a function of the ignition delay time over a wide range of conditions. Our results demonstrate the potential of the sparse-learning approach as an effective and efficient tool for dynamical system analysis and reduction. The uniqueness of this approach as applied to combustion systems lies in the ability to identify influential reactions in specified conditions and times during the evolution of the combustion process. This ability is of great interest to understand chemical reaction systems.

Keywords: Sparse identification, Mechanism reduction, Reaction elimination, Sparse learning

1. Introduction

Extracting underlying dynamics from noisy measurement data is a key challenge in several areas of science and engineering, such as system identifi-

cation of distillation columns [1], computational neuroscience [2], stock-price prediction [3], climate modeling [4], and chemical reaction network modeling [5]. This work presents an optimization-based method that is comprised of hybrid data-driven models (black-box) and mechanistic state space models (white-box) based on sparsity techniques to study combustion reaction networks.

Combustion is a ubiquitous process with applications that vary extensively, ranging from heating and transportation to mass production of metallic and ceramic nanoparticles. It involves different processes that span a wide range of length and time scales, and are controlled by the delicate interplay among several chemical and physical phenomena, such as chemical kinetics, thermodynamics, fluid mechanics, and heat transfer. Over the past decades, chemical modeling has played a great role due to the continuing expansion in computational capabilities, development of diagnostic methods, quantum chemistry methods and kinetic theory. Within this context, the approach to developing detailed kinetic models (mechanisms) of fuel combustion involves compiling a set of elementary reactions whose rate parameters may be determined from individual rate measurements, reaction-rate theory, or a combination of both. These detailed mechanisms consist of a large number of chemical species and reactions: for example, the mechanisms of large hydrocarbons, as the ones used in surrogates for real transportation fuels, typically describe the interactions of $\sim 10^2 - 10^3$ species via $10^3 - 10^4$ reactions [6]. The resulting networks of reactions show high nonlinearity and dimensionality. The relevance of the different species and reactions not only changes with time during combustion, but also depends on the specific system and

conditions (*e.g.*, temperature, pressure, equivalence ratio).

The analysis of chemical kinetic mechanisms, particularly understanding the relevance of different species and reactions in various conditions, has several important applications. While chemical mechanisms have been active research area for last several decades, refinements in implemented pathways and reaction rate parameters are still necessary. Thus, in exploratory chemical synthesis, such as design of more efficient fuels or pharmaceuticals, the identification of the most influential reactions in the network provides critical information on the chemical mechanisms that might be targeted in the design. The analysis of chemical reaction networks can be leveraged to generate reduced chemical mechanisms that have similar combustion characteristics to the parent mechanism but present a significantly smaller number of species and reactions. A direct application of this work is the use of reduced mechanisms into computational fluid dynamics simulations to describe realistic combustion systems like engines, overcoming the complexity and computational cost of large kinetic mechanisms that make full kinetic models unusable in most cases [7–9]. For example, computational simulations of internal combustion engines require the coupling of chemical models for the conversion of the fuel into combustion products with numerical treatments of the fluid dynamics of reacting flows [6]. Evaluating the influence of each species or reaction on the combustion process is a widely used strategy for developing reduced kinetic mechanisms [7, 8, 10–19].

In this paper, we propose a different approach based on the use of data-driven sparse-learning methods to analyze reaction mechanisms and identify the most influential reactions. The data-driven approach simplifies complex

nonlinear dynamical models to scalable linear models; the sparse-learning methodology removes weak interdependencies within the reaction network and creates a sparse network. The uniqueness of this approach as applied to combustion systems lies in the ability to identify influential reactions in specified conditions and times during the evolution of the combustion process. Majority of methods introduced in the literature for mechanism reduction consider the entire process and are not capable of identifying the active reactions under certain conditions and at certain times during the evolution of process [15, 18]. The set of active reactions at each time is a small subset of reduced mechanism delivered by those methods. One of the outcomes of the proposed method is the set of influential reactions under each condition and at each sampled time. Additionally, unlike other methods in the literature, such as the perturbation sensitivity analysis [20–22], integer linear programming based elimination [15], and error propagation based directed relation graph (DRGEP) [18], the proposed method does not require any understanding of the underlying chemical process, instead it learns from data generated from the chemical process. The proposed method is applied to the analysis of two mechanisms describing the chemistry of H_2 fuel and C_3H_8 fuel, respectively. We also demonstrate how this new method can be used to derive a reduced version of the parent chemical mechanism without the need for additional simulations, making it considerably more efficient compared to other equivalent methods. By finding a set of influential reactions using species concentrations and reaction rates, the proposed method is not biased toward any specific combustion property [23].

2. Methodology of Sparse Identification

2.1. Model Framework for Sparse Identification

In this study, we consider sparse identification of discretized dynamical systems of the form, given by:

$$\mathbf{X}_{t+1} = f(\mathbf{X}_t) + g(\mathbf{r}_t)\Delta_t + \boldsymbol{\omega}_t, \quad t = 1, 2, \dots, T - 1, \quad (1)$$

where \mathbf{X}_t is an $N_1 \times 1$ vector that represents states of the dynamical system at time t , \mathbf{r}_t is an $N_2 \times 1$ vector that denotes the actuation (control action) at time t , Δ_t is the discrete step-size, and $\boldsymbol{\omega}_t$ represents the modeling error. The problem of sparse identification is equivalent to finding the most significant set of actuators such that the reduced dynamical model with sparsely placed actuators closely approximate the full-scale model with all actuators in place.

To that end, we define a selection/weight vector $\mathbf{w}_t = [w_{1,t}, w_{2,t}, \dots, w_{N_2,t}]^\top$, which represents the binary weights of all the actuators at time t . Thus, \mathbf{w}_t selects a subset of all the actuators to describe evolution of the sparse dynamical system. Correspondingly, an error is introduced in the states of the system, described by

$$\mathcal{E}_t(\mathbf{w}_t) = |\mathbf{X}_{t+1} - f(\mathbf{X}_t) - g(\mathbf{w}_t \odot \mathbf{r}_t)\Delta_t|, \quad (2)$$

where \odot denotes the element-wise product. Based on these definitions, we can impose a constraint on the identification error of each state at all times as

$$\mathcal{E}_{j,t}(\mathbf{w}_t) \leq \epsilon |g(\mathbf{r}_t)|(j)\Delta_t, \quad \forall t, \forall j \in \{1, \dots, N_1\}, \quad (3)$$

where ϵ is a tuning parameter that indicates the acceptable error tolerance of $|g(\mathbf{r}_t)|$. In order to solve this problem, we formulate the following mathe-

mathematical approach to data-driven sparse identification:

$$\{\mathbf{w}_k^*\}_{k=1}^{T-1} = \underset{\{\mathbf{w}_k\}_{k=1}^{T-1}}{\text{minimize}} \sum_{k=1}^{T-1} \sum_{i=1}^{N_2} \mathbf{w}_{i,k} \quad (P_{\text{Sparse Identification}})$$

subject to $\mathbf{w}_{i,k} \in \{0, 1\}$, $i = 1, 2, \dots, N_2$,

Eqs. 3 holds.

2.2. Application to Chemical Reaction Networks

The time evolution of a reactive system is commonly modeled using mass-action kinetic equations [24–28], which, by applying Euler discretization method [29], can be written as

$$\mathbf{X}_{t+1} = \mathbf{X}_t + \mathbf{M}\mathbf{r}_t\Delta_t + \boldsymbol{\omega}_t, \quad t = 1, 2, \dots, T - 1, \quad (4)$$

where \mathbf{X}_t is an $N_s \times 1$ vector of concentrations of all the N_s species at time t , N_r is the number of reactions whose stoichiometric coefficients are contained in the $N_s \times N_r$ matrix \mathbf{M} , Δ_t is the sampling time used for discretization, and $\boldsymbol{\omega}_t$ denotes the discretization error and process noise. Finally, \mathbf{r}_t is the $N_r \times 1$ vector of the rates of N_r reactions, which can be expressed as:

$$\mathbf{r}_t(i) = k_i \prod_{j=1}^{N_s} \mathbf{X}_t(j)^{\nu_{ij}}, \quad (5)$$

where k_i is the rate constant for the i^{th} reaction, $\mathbf{X}_t(j)$ denotes the j^{th} component of \mathbf{X}_t , and ν_{ij} are the stoichiometric coefficients for the reactants of reaction i and zero otherwise. Note that the discretized mass-kinetic equation resembles the dynamical model in (1) with appropriate choices of functions $f(\cdot)$ and $g(\cdot)$.

For each reaction, we introduce a selection (binary case) variable $w_{i,t}$, which describes the significance of the i^{th} reaction at time t (value of 1

corresponds to more influential reaction), and the selection vector $\mathbf{w}_t = [w_{1,t}, w_{2,t}, \dots, w_{N_r,t}]^\top$, which represents the selection of all the reactions at time t .

Similar to (2), an error is introduced in the concentration of the species that can be expressed for the j^{th} species as

$$\mathcal{E}_{j,t}(\mathbf{w}_t) = |\mathbf{X}_{t+1}(j) - \mathbf{X}_t(j) - \mathbf{M}_j(\mathbf{w}_t \odot \mathbf{r}_t)\Delta_t|, \quad (6)$$

where \mathbf{M}_j denotes the j^{th} row of matrix \mathbf{M} and \odot denotes the element-wise product. Based on these definitions, we can impose a constraint on the concentration error of each species at all times as

$$\mathcal{E}_{j,t}(\mathbf{w}_t) \leq \epsilon \mathcal{N}_t(j), \quad \forall t, \forall j \in \{1, \dots, N_s\}, \quad (7)$$

$$\mathcal{N}_t(j) = |\mathbf{M}_j| \mathbf{r}_t \Delta_t, \quad j \in \{1, \dots, N_s\}. \quad (8)$$

where \mathcal{N}_t is a normalization factor at time t , defined as the sum of absolute changes in all concentrations at time t , and ϵ is a tuning parameter that indicates the acceptable error tolerance of \mathcal{N}_t , *e.g.*, $\epsilon = 0.05$ enforces a maximum of 5% error.

The constraint introduced in Eq. 7 is effective against the addition of noise in the concentration evolution but is not very effective in limiting constant drifts in the species concentration. To correct for this issue, we added an additional constraint to limit the propagation of error over time. For the change in concentration of the j^{th} species in time horizon $\{t, t+1, \dots, t+H-1\}$, we have that

$$|\mathbf{X}_{t+H-1}(j) - \mathbf{X}_t(j) - \sum_{k=t}^{t+H-2} \mathbf{M}_j(\mathbf{w}_k \odot \mathbf{r}_k)\Delta_k| \leq \beta \epsilon \sum_{k=t}^{t+H-2} \mathcal{N}_k(j), \quad (9)$$

where H is the number of time samples $\{t, t+1, \dots\}$ in the time horizon $[t, t+H-1]$ and β is a tuning parameter that limits the amount of concentration drift. Intuitively, larger H enforces error toleration bound on a longer time period and results in having more reactions in the reduced mechanism. For the choice of H , two points should be considered:

1. *Physical effect*: larger choice of H enforces the aggregated error in the concentrations of all species that is caused by removing some of the reactions to remain in the acceptable range for a larger time horizon. On the other hand, the choice of smaller H , relaxes the propagated error to be in the same range, but for a smaller time horizon. Consequently, the larger H results in a reduced mechanism with more reactions.
2. *Computational cost*: larger H results in less number of optimization problems of larger size, and smaller choice of H creates more optimization problems of smaller size. The effect of H on the number of variables in the optimization is illustrated in Table 1.

2.2.1. Sparse-Learning Reaction Selection (SLRS) method

The task of finding the most influential reactions is a matter of determining the smallest subset of reactions that are active at any given time, such that the error in the concentrations induced by limiting the number of reactions remains in a user-specified tolerance range (ϵ, β) at all times.

To solve this problem, we formulated the following mathematical approach to data-driven sparse-learning reaction selection. For each time batch

of size H , we solve the following integer linear programming (ILP) problem:

$$\begin{aligned} \{\mathbf{w}_k^*\}_{k=t}^{t+H-1} = \underset{\{\mathbf{w}_k\}_{k=t}^{t+H-1}}{\text{minimize}} & \sum_{k=t}^{t+H-1} \sum_{i=1}^{N_r} \mathbf{w}_{i,k} & (P_{SLRS}) \\ \text{subject to} & \mathbf{w}_{i,k} \in \{0, 1\}, \quad i = 1, 2, \dots, N_r, \\ & \forall k \in \{t, t+1, \dots, t+H-1\} \\ & \text{Eqs. 7,9 hold.} \end{aligned}$$

where $\{\mathbf{w}_k\}_{k=t}^{t+H-1}$ are binary-valued optimization variables. Note that solving problem (P_{SLRS}) delivers the minimum number of reactions such that the error tolerance constraints on individual concentrations (Eq. 7) and on error propagation (Eq. 9) are satisfied.

To further reduce the complexity of our data-driven sparse-learning approach, we can use convex relaxation methods [30] by replacing the binary variable constraint with its convex hull, *i.e.*, $0 \leq \mathbf{w}_{i,t} \leq 1$ for all i . The relaxed problem has the following form:

$$\begin{aligned} \{\mathbf{w}_k^*\}_{k=t}^{t+H-1} = \underset{\{\mathbf{w}_k\}_{k=t}^{t+H-1}}{\text{minimize}} & \sum_{k=t}^{t+H-1} \sum_{i=1}^{N_r} \mathbf{w}_{i,k} & (P_{RSLRS}) \\ \text{subject to} & 0 \leq \mathbf{w}_{i,k} \leq 1, \quad i = 1, 2, \dots, N_r, \\ & \forall k \in \{t, t+1, \dots, t+H-1\} \\ & \text{Eqs. 7,9 hold.} \end{aligned}$$

This relaxation of (P_{SLRS}) yields a linear programming problem. The complexity of this linear programming relaxed formulation grows linearly with the number of reactions in the full mechanism and can be solved in polynomial time. This makes our approach promising for large-scale chemical reaction networks at the cost of losing optimality guarantees. Moreover, the

solution of (P_{RSLRS}) \mathbf{w}_i^* is a real-valued vector, which is more informative but not immediately suitable for the selection of a subset of reactions. In order to project this solution onto a binary vector, we set a threshold as follows

$$\begin{cases} \tilde{\mathbf{w}}_{i,k} = 1 & \text{if } \mathbf{w}_{i,k}^* > \alpha \\ \tilde{\mathbf{w}}_{i,k} = 0 & \text{if } \mathbf{w}_{i,k}^* \leq \alpha \end{cases}, \quad (10)$$

where α is a threshold value and $\tilde{\mathbf{w}}$ is in the form of a selection vector similar to the solution of problem (P_{SLRS}) .

The next step is to find the reduced mechanism not just for the time horizon $[t, t + H - 1]$, but for the entire sampled interval $[0, t_f]$, where t_f is the last time sample. In order to do this, we solve problem (P_{RSLRS}) for time intervals $[0, H - 1], [H, 2H - 1], \dots, [KH, t_f]$, where KH is the largest integer multiple of H that is smaller than or equal to t_f , as described in Algorithm 1. The output of Algorithm 1 is a matrix $\mathbf{W}(\theta)$, with columns indicating the selected reactions at each time instance under specific initial conditions, namely temperature T , equivalence ratio ϕ , and pressure P (*i.e.*, $\theta = [T, \phi, P]$).

2.2.2. Complexity Analysis and Computational Cost

The original problem (P_{SLRS}) is a standard ILP problem, and thus can be solved using state-of-the-art ILP solvers such as Gurobi [31] and CPLEX [32]. Even though these solvers can solve problems with large numbers of integer variables relatively fast by employing branch and bounding algorithms, the worst-case complexity of ILP is exponential in the number of integer variables. On the other hand, the relaxed problem (P_{RSLRS}) is a linear programming (LP) problem, which can be solved in polynomial time. Table 1 lists

Algorithm 1 Calculating $\mathbf{w}(\theta)$

Input: $\{\mathbf{X}_t\}_{t=0}^{t_f}$, $\{\mathbf{r}_t\}_{t=0}^{t_f}$, $\{\Delta_t\}_{t=1}^{t_f}$, ϵ , β , $\theta = [\phi, T, P]$, \mathbf{H} , \mathbf{M} Initialize: $t = 0$, $\mathbf{w}_{-1} = \mathbf{0}$, $\mathbf{W}(\theta) \in \mathbb{R}^{N_r \times N_t}$.

1. While ($t \leq t_f$)
 - $W = \min\{H, t_f - t + 1\}$.
 - set the time horizon to $[t, t + W - 1]$.
 - solve problem (P_{RSLRS}) to obtain $\mathbf{w}_t^*, t \in [t, t + W - 1]$.
 - Assign $\mathbf{w}_t^*, t \in [t, t + W - 1]$ values to columns $[t, t + W - 1]$ of $\mathbf{W}(\theta)$.
 - $t + W \rightarrow t$.
 - End while
 2. Return $\mathbf{W}(\theta)$ or $\mathbf{w}_t^*, t \in [0, t_f]$.
-

the factors (*i.e.*, variables and constraints) that affect the performance of the two approaches.

Table 1: Complexity analysis for each optimization problem with time horizon of size H

	Real variables	Integer variables	Linear constraints	Integral constraints
P_{SLRS}	0	$N_r H$	$N_r H$	$2N_s(H + 1)$
P_{RSLRS}	$N_r H$	0	$2N_s(H + 1) + 3N_r H$	0

The performance of the integer programming solution and the relaxed linear programming solution are compared in Tab. 2. These run-time values are calculated by taking the average of the times it takes to run Algorithm 1

(with the corresponding formulation) for different values of θ . The results show that solving the relaxed formulation (P_{RSLRS}) significantly reduces the computational cost to less than $\frac{1}{5}$ th of the integer formulation. It should be noted that both methodologies can easily be accelerated via parallelization, as each initial condition θ can be analyzed independently. Since the original problem (P_{SLRS}) has a worst-case exponential complexity, the rest of this paper focuses on the relaxed problem.

Table 2: Comparison of computational performances of P_{SLRS} and P_{RSLRS} on 48 Hydrogen mechanism simulations and 216 Propane mechanisms with different initial conditions.

		Average (core s)	Total (core hr)	H	# problems
Hydrogen	P_{SLRS}	0.055	8.33e-4	20	384
Hydrogen	P_{RSLRS}	0.059	7.92e-4	20	384
Propane	P_{SLRS}	2273	136.38	20	1944
Propane	P_{RSLRS}	394	23.64	20	1944

The total analysis time for 48 H₂/air system simulations using sparse learning reaction selection approach is 2.99 seconds. All the calculations are performed on a Linux based machine with a 2.1 GHz processor and 8 GB of RAM.

3. Analysis of H₂/air system

As the first system of investigation, we used the proposed relaxed SLRS approach to study the combustion of H₂ in air. Hydrogen combustion is chosen because it yields one of the smallest reaction networks in combustion

(8 species and 62 reactions counting both forward and reverse processes [33]) and is a well-studied system.

Constant-volume, homogeneous reactor simulations, performed with Ansys Chemkin [34] and a H_2 oxidation mechanism by Hong et al. [33], were used to create the reference chemical reaction network for two different initial conditions ($P = 20$ atm, $T = 900$ K, $\phi = 1, 2$). For each condition, we identified the influential reactions using SLRS parameters of $\epsilon = 0.21$, $\beta = 3$, and $\alpha = 0$, and the results of five sampling regions are shown in Fig. 1.

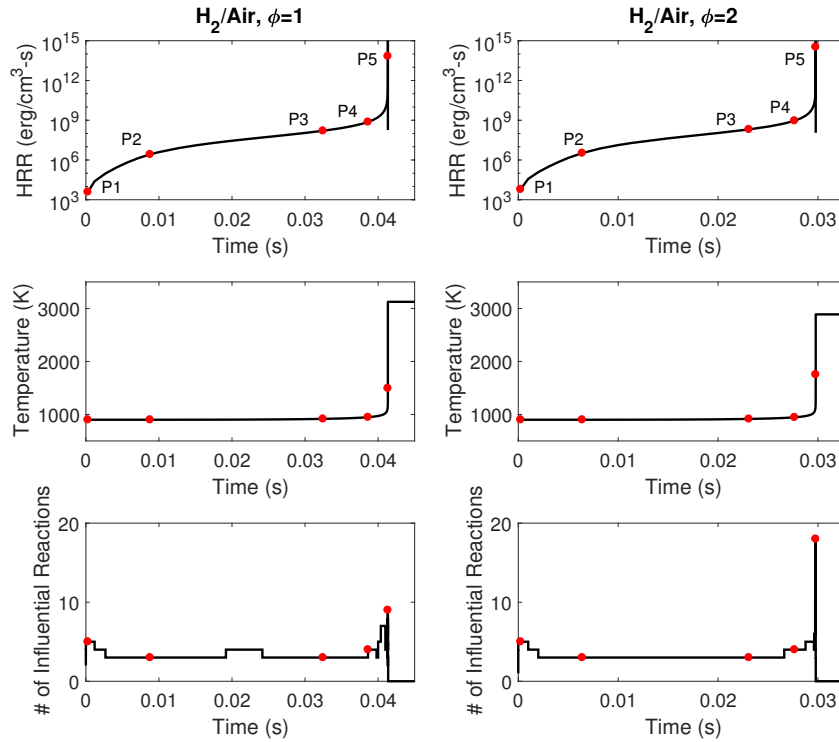


Figure 1: Calculated heat release rates (HRR), temperature profiles, and the number of influential reactions for H_2/air mixture with the initial condition of 20 atm and 900 K. Highlighted are five points (P1-P5) during the time evolution.

The analysis of the results, listed in Table 3, shows that the set of influential reactions prior to the ignition time is identical for both stoichiometric and fuel-rich cases. Initially at P1, the algorithm identifies reactions that consume the fuel as well as three-body reactions generating HO₂ as influential. As the ignition process progresses (from P2 to P3), reactions associated with HO₂ production/consumption become prominent, with a shift in the H₂O₂ production pathway from H₂ + HO₂ to recombination of two HO₂ radicals, likely due to increased concentration of HO₂ radicals. As the system is approaching ignition (P4), the relaxed model introduces an additional influential reaction pathway that leads to the formation of OH.

Once ignition is reached (P5), we observe a difference between the two systems in influential reactions. Interestingly, influential reactions from the stoichiometric case are a subset of the ones from the fuel-rich case. In both cases, the algorithm selects chain branching reactions (*e.g.*, H + O₂ → O + OH, H₂ + O → H + OH) that are well-known factors for onset of high-temperature ignition as well as reactions that are associated with HO₂ and water formation. In addition to these reactions, under fuel-rich conditions, nine more reactions are identified including three H₂ formation reactions from H radical, which describe the dynamic equilibrium between H radical and remaining H₂.

The time evolution of the influential reactions identified by the proposed algorithm described above agrees well with the general understandings of the ignition of hydrogen as discussed in the literature [33, 35]. For example, when the temperature is lower than 900 K (P1 to P4), the proposed algorithm correctly identifies the preferential pathway to produce HO₂ from H + O₂

instead of the chain branching pathway that generates $O + OH$, which is important only at higher temperatures. Moreover, the proposed algorithm correctly captures the dominance of fuel consumption reactions during the very early phase, as well as the reactions that lead to ignition at the ignition time (H_2O_2 dissociation, chain propagation/branching reactions for HO_2).

As the proposed sparse-learning approach is designed to identify the influential reactions of a combustion process, it can be leveraged to generate a reduced mechanism, *i.e.*, a coarser reaction network of the analyzed mechanism. Even though, H_2 mechanism is a small mechanism and its reduction is not a practical problem, our results highlight the capability of the algorithm to produce a reduced mechanism that includes almost half of the reactions, and that still accurately reproduce the results of the parent mechanism under a wide variety of initial conditions.

To this end, we generated and analyzed 48 homogeneous reactor constant-volume simulations of H_2 /air combustion with initial conditions between 5–20 atm, 800–1100 K, and equivalence ratios between 0.5–2. From these simulations, we selected the union of the influential reactions identified for each initial condition at each time, obtaining a set of 31 reactions. The ignition delay times in constant-volume simulations for the reduced mechanism were compared against those obtained using the full mechanism.

Figure 2 shows the percentage deviation in ignition delay time from the full H_2 mechanism for selected conditions. The results which are representative of all the tested conditions, show that the differences in ignition delay time are well below 2% for the reduced mechanism over a wide range of conditions, despite the significantly smaller number of reactions compared to the

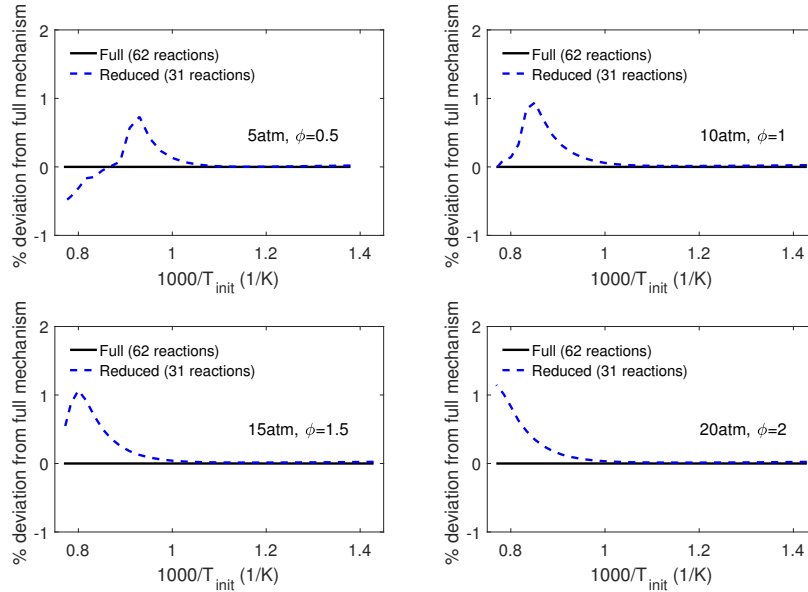


Figure 2: Ignition delay time deviation from the full mechanism for H_2/air mixture.

full mechanism (31 vs 62 reactions). The maximum deviation occurs when the initial temperature is above 1000 K, while low-temperature ignition delay times are nearly identical to the full mechanism. Overall, the excellent reproducibility of the ignition delay time (less than 2% over all the conditions) indicates that the proposed method is a very effective approach to build a reduced mechanism that performs well in a wide range of thermodynamic conditions. Moreover, it demonstrates that the ignition delay time, which is one of the most important combustion characteristics in practical energy conversion devices, can be preserved with the proposed method even if it is not explicitly taken into account directly during the reduction process.

4. Analysis of Propane Combustion

As a second application of the proposed sparse-learning approach, we analyzed the network of reactions describing the chemistry of propane. We used the full mechanism by Petersen et al. [36], which includes 117 species and 1270 reactions. Similar to the hydrogen case described in the previous section, we used a 0-D reactor for the simulation of a stoichiometric propane/air mixture at 20 atm and 700 K. This system was chosen to identify the reactions that are responsible for the two-stage ignition behavior, a distinctive low-temperature ignition characteristics of alkanes.

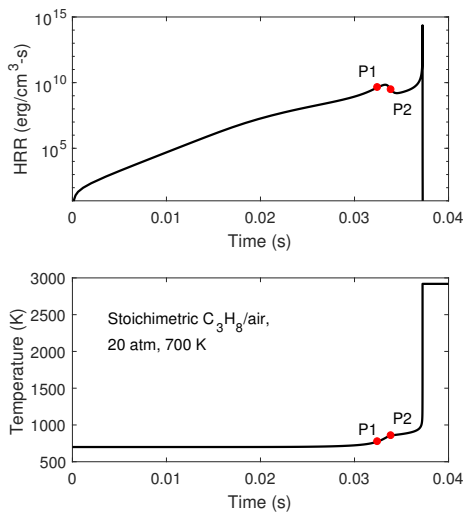


Figure 3: Calculated heat release rate (HRR) and temperature of stoichiometric propane/air mixture with the initial condition of 20 atm and 700 K.

Fig. 3 reports the calculated heat release rate and temperature profile for this system. The two-stage behavior is highlighted by the peak of heat release rate and subsequent decrease (0.03 – 0.035 s) before the ignition

occurs (~ 0.0372 s). This trend is generally associated with the competition between different low-temperature pathways (see Fig. 4 for a scheme of the major low-temperature pathways in alkane mechanisms [37–41]).

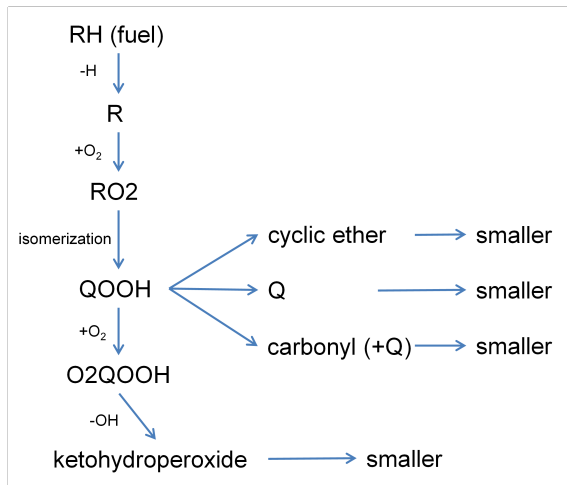


Figure 4: Schematic of major low-temperature oxidation pathways for alkanes.

At low temperatures, once hydroperoxy alkyl radicals (QOOH) are initially formed, the pathway to ketohydroperoxides via second O_2 addition ($QOOH \longrightarrow O_2QOOH \longrightarrow \text{ketohydroperoxide}$) is favored. However, as temperature increases during the ignition process, other pathways (*i.e.*, $QOOH \longrightarrow Q$ or carbonyl or cyclic ether) become increasingly relevant and dominate the low-temperature reactivity. As olefins (Q) and carbonyl radicals are more stable than ketohydroperoxides in such conditions, the charge reactivity and heat release rate slightly decrease as shown above.

To test if this behavior is captured by the proposed algorithm, we analyzed the system ($\epsilon = 0.5$, $\beta = 3$, $\alpha = 0$) at two different times, namely, before (P1) and after (P2) the peak heat release rate point as shown in Fig. 3. Out of 1270 reactions in the mechanism, the algorithm identified 68 influ-

ential reactions at P1 and 49 influential reactions at P2, with most of the differences between the two sets occurring in the low-temperature chemistry reactions, which are listed in Table 4. The algorithm correctly identifies reactions in both groups of pathways as influential at P1, while at P2 the pathway to ketohydroperoxide is omitted and only the reactions that lead to Q or carbonyl production (less reactive pathway) are selected as influential.

Since our approach was able to capture the low-temperature behavior of propane combustion, we analyzed the differences between low ($\phi = 1$, 700 K, 20 atm, simulated above) and high temperatures ($\phi = 1$, 1500 K, 20 atm) combustion using the same parameters as before ($\epsilon = 0.5$, $\beta = 3$). To simplify the comparison, we added an additional constraint to the optimization problem to accumulate the selection of influential reactions over the duration of each simulation.

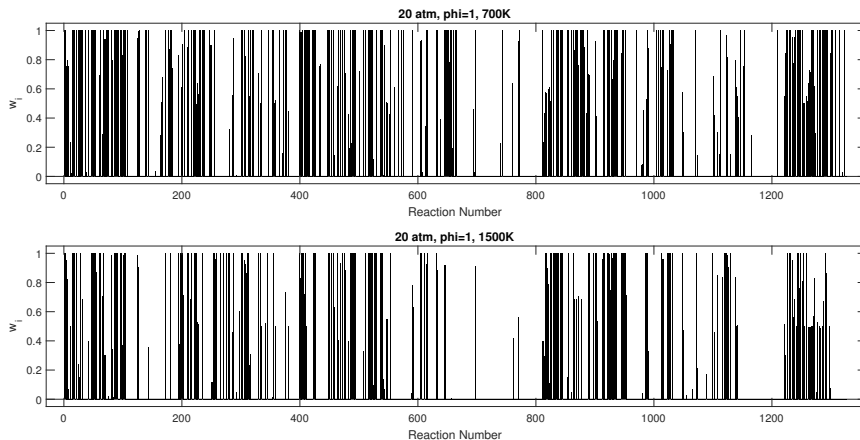


Figure 5: Relevance (measured by the weight w_i) of the reactions from propane ignition simulations.

Figure 5 shows the relevance of each reaction in both conditions, as increasing values of w_i correspond to more influential reactions. The reactions are labeled by using an incremental number obtained by listing forward and reverse reactions in the same order they are presented in the original mechanism. For example, the first reaction in the parent mechanism is $\text{H} + \text{O}_2 \rightleftharpoons \text{O} + \text{OH}$, which becomes reaction 1 ($\text{H} + \text{O}_2 \longrightarrow \text{O} + \text{OH}$) and 2 ($\text{O} + \text{OH} \longrightarrow \text{H} + \text{O}_2$) in the abscissa of Figs 5 and Figs 6. From the comparison of the two plots, we find that the algorithm identifies more influential reactions ($\alpha = 0$) for the low-temperature system (420) than for the high-temperature one (350). This trend is expected, as the former system needs to include reactions from the low-temperature regime in addition to the high-temperature reactive pathways, which is in agreement with other works presented in the literature [19, 42]. The detailed comparison between the two sets of reactions can also provide useful insights on the low-temperature chemistry. For example, most of the reactions between 647–664, which describe hydrogen abstractions from $\text{C}_2\text{H}_3\text{CHO}$ by various radicals, are identified as influential only for the 700 K case. The analysis of the mechanism indicates that $\text{C}_2\text{H}_3\text{CHO}$ is predominantly associated with the low-temperature chemistry including RO_2 and O_2QOOH elimination pathways, *e.g.*, $\text{QOOH} \longrightarrow \text{Q} \longrightarrow \text{smaller}$. Similarly, reactions between 1301–1326, which represent decomposition pathway of C3 carbonyl compounds ($\text{C}_3\text{H}_6\text{O}_1\text{-2}$, $\text{C}_3\text{H}_6\text{O}_1\text{-3}$), are irrelevant for the high-temperature system while some of them are influential for the 700 K case. As these C3 carbonyls are mostly created by QOOH chemistry, pathways that are well-known to be associated with low-temperature conditions, we find again that the algorithm selection

matches our understanding of this kinetic mechanism.

To create a list of influential reactions a cutoff (α) for w_i (see Eq. 10) is required. However, directly comparing the values of w_i in their multireaction context is more informative. For example, if we analyze in detail the reactions between 1235–1288 (shown in Fig. 6) that represent several low-temperature reactions (*e.g.*, $\text{RO}_2 \longrightarrow \text{QOOH}$, QOOH destruction pathways, $\text{QOOH} + \text{O}_2 \longrightarrow \text{O}_2\text{QOOH} \longrightarrow \text{KET} \longrightarrow \text{smaller}$, $\text{O}_2\text{QOOH} \longrightarrow \text{smaller}$), we can see that while almost all the reactions have $w_i > 0$, their relevance (w_i) changes in the two systems. In this way, it is straightforward to identify the reactions that are relevant in both regimes (*e.g.*, 1245) or reactions that are prevalent in a specific regime (*e.g.*, 1259 or 1267), particularly for complex and larger reaction networks, for which the assessments of relative importance among different pathways for specific combustion behavior is very challenging.

Using a similar approach as for the H_2 mechanism study, we assembled a reduced mechanism for the propane chemistry. To formulate a reduced mechanism that works in both low-/high-temperature regime, we analyzed influential reactions identified from 216 conditions (700–1500 K, 1–50 atm, and equivalence ratios of 0.5–2) from homogeneous reactor simulations. The performances of the reduced version of the propane mechanism, which consists of 111 species and 691 reactions, were again tested by comparing ignition delay times with the ones predicted by the parent mechanism. The results, of which a representative sample is shown in Fig. 7, show that ignition delay times predicted by the reduced mechanism are within 40% of those by the parent propane mechanism and that the NTC (negative temperature coeffi-

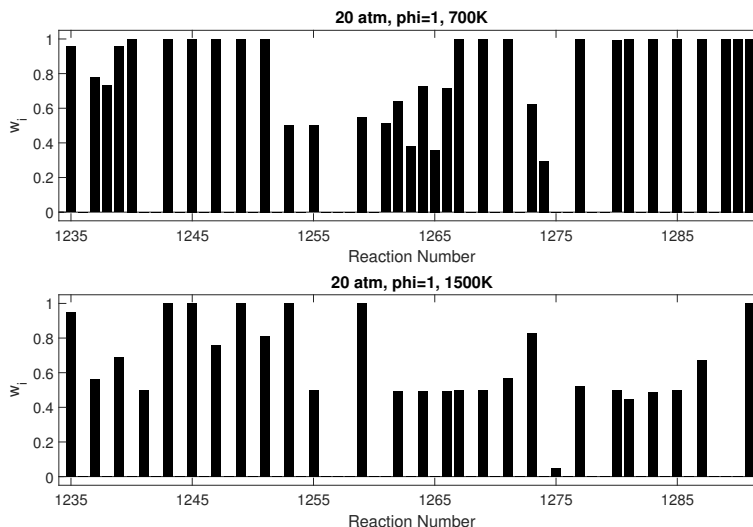


Figure 6: Magnification of the importance (measured by the weight w_i) of the propane ignition reactions shown in Fig. 5.

cient) behavior predicted by the parent mechanism is preserved.

4.1. Comparison with Other Methods

For comparison, we applied the brute force sensitivity analysis to reduce the propane mechanism at one of the 216 conditions (700K, 20 atm). Due to the excessive computation time required for the sensitivity analysis method, we only tested the method at just one condition. For the sensitivity analysis method, the change in ignition delay time due to elimination of each reaction is quantified and the reaction that caused smallest change is eliminated. This process was iterated until the change in ignition delay time is smaller than 40% while achieving reasonable post-ignition temperature ($\pm 50K$).

As a result, the sensitivity analysis method resulted in 113 species and 641 reactions. While this method successfully maintained the ignition delay

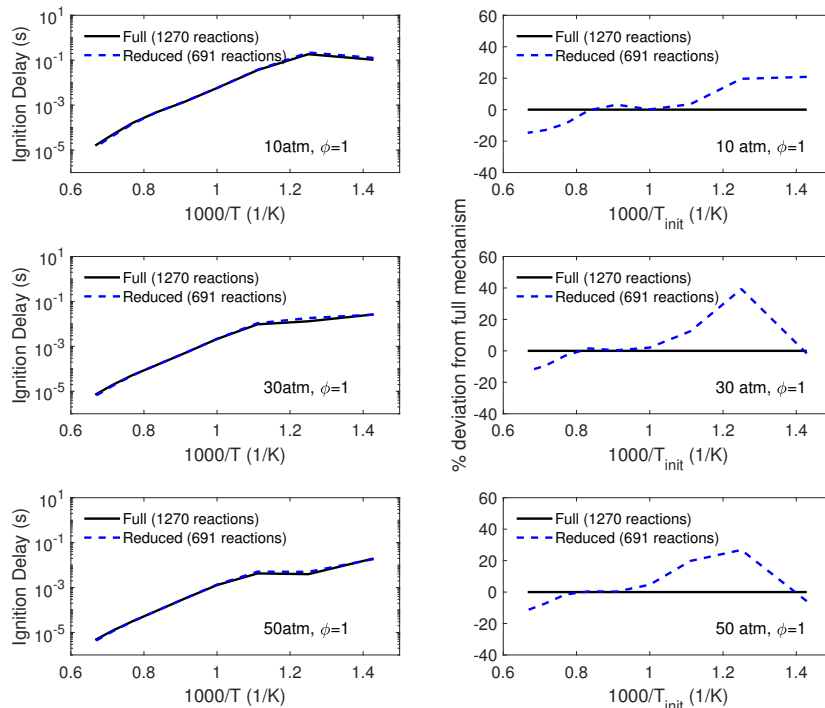


Figure 7: Comparisons of computed ignition delay times using the full and reduced mechanisms for stoichiometric propane/air mixture at 10 atm, 30 atm, and 50 atm

trend and shows similar level of reduction in terms of the number of reaction, it requires significantly more computational time when compared to the proposed sparse learning method. Performing one set of sensitivity analysis requires ignition calculations at each chosen initial condition with removing each reaction one by one. Even for the test case with a single initial condition, performing one set of sensitivity study to remove one reaction requires more than 1000 ignition calculations (same as the number of reactions) which took in the order of 10 minutes with 8 parallel runs. Thus, to reach the current result, the sensitivity study needed about 100 hours. If all 216 conditions

are to be included, approximately 216 x 100 hours might be needed, which is prohibitively long and harms its applicability to large mechanisms relevant to practical fuels.

In addition, we also generated a reduced mechanism using the DRGEP method [18] for the same 216 conditions (temperature/pressure/equivalence ratio) considered above. We set the ignition delay threshold of the DRGEP method at 40% to match the maximum deviation observed for our reduced mechanism and the resulting mechanism consisted in 81 species and 885 reactions. While both reduced mechanisms generated by the proposed sparse learning and DRGEP successfully maintained the ignition delay trend, the number of species and reactions in the reduced mechanisms highlight the substantial differences in their approaches. DRGEP prioritizes decreasing the number of species which automatically eliminates all reactions containing the removed species. While a modified implementation of DRGEP [18] does allow for the ranking of reactions with respect to influence on a target species, the proposed sparse learning method has the advantage of analyzing the importance of each reaction one by one as part of the entire reaction system. In practice, DRGEP has often been combined with a second reduction method such as quasi-steady state [18], principal component analysis [43], or sensitivity [19] analysis to provide additional reduction. Thus, it may be more beneficial in the future to develop a hybrid approach that combines the unique data-driven upside of our sparse learning with DRG-type methods to maximize the level of reduction.

5. Conclusions

In this work, we present a new method for sparse identification of dynamical systems with emphasis on analyzing complex chemical reaction networks by employing a data-driven sparse-learning approach. Using concentration and reaction rates at a given time, the proposed optimization approach is able to identify the most influential reactions in the network, that is the smallest subset of reactions that is able to approximate the concentration of the species to within a prescribed error tolerance using a convex relaxation method to solve the underlying optimization problem. The proposed approach has the following advantages: guaranteed concentration approximation accuracy over all time points; low computational cost; and versatility due to its applicability to general chemical reaction networks.

We tested our approach on reaction networks generated by the combustion of two fuels, hydrogen and propane. When applied to the H_2 combustion, our method was able to identify the key reactions that mark the different phases of the ignition process. Moreover, a reduced mechanism of the H_2 oxidation is built by collecting the influential reactions at all times in a wide range of thermodynamic conditions (5–20 atm, 800–1100 K, $\phi = 0.5$ –2), displayed a deviation from ignition delay time of less than 2%, while using only half of the reactions.

The analysis of the C_3H_8 combustion mechanism showed that our method can identify the changes in low-temperature pathways and capture the propane’s characteristic two-stage ignition behavior, as well as the differences in relevant reactions between low- and high-temperature ignition conditions. Similarly to hydrogen combustion, we built a reduced mechanism consisting of

111 species (reduced by 5.1%) and 691 reactions (reduced by 45.6%), by analyzing the combustions of 216 different systems. The ignition delay times obtained with the reduced mechanism are within 40% deviation of the original mechanism in a wide range of conditions (700–1500 K, 1–50 atm, $\phi = 0.5$ -2).

This study showcases the potential of the proposed data-driven approach to analyze very complex reaction networks and to perform mechanism reduction in a computationally-efficient manner.

Acknowledgments

This research has been funded by the US Army Research Office grants W911NF-15-1-0241 and W911NF-14-1-0359. PE and AV thank the College of Engineering at the University of Michigan for partially supporting this work.

References

- [1] R. Subramanian, S. Singh, Can machine learning identify governing laws for dynamics in complex engineered systems?: A study in chemical engineering, arXiv preprint arXiv:1907.07755 (2019).
- [2] P. D. Maia, J. N. Kutz, Identifying critical regions for spike propagation in axon segments, *Journal of computational neuroscience* 36 (2014) 141–155.
- [3] D. P. Kuttichira, E. Gopalakrishnan, V. K. Menon, K. Soman, Stock price prediction using dynamic mode decomposition, in: 2017 International Conference on Advances in Computing, Communications and Informatics (ICACCI), IEEE, 2017, pp. 55–60.

- [4] H. A. Kingravi, H. R. Maske, G. Chowdhary, Kernel observers: Systems-theoretic modeling and inference of spatiotemporally evolving processes, in: *Advances in Neural Information Processing Systems*, 2016, pp. 3990–3998.
- [5] S. Burnham, M. Willis, A. Wright, Identifying chemical reaction network models, *IFAC Proceedings Volumes* 40 (2007) 225–230.
- [6] C. K. Law, Combustion at a crossroads: Status and prospects, *Proceedings of the Combustion Institute* 31 (2007) 1–29.
- [7] A. S. Tomlin, T. Turányi, M. J. Pilling, Chapter 4 Mathematical tools for the construction, investigation and reduction of combustion mechanisms, in: M. J. Pilling (Ed.), *Comprehensive Chemical Kinetics*, volume 35 of *Low-Temperature Combustion and Autoignition*, Elsevier, New York, 1997, pp. 293–437.
- [8] T. Turányi, Sensitivity analysis of complex kinetic systems. Tools and applications, *Journal of Mathematical Chemistry* 5 (1990) 203–248.
- [9] T. Lu, C. K. Law, Toward accommodating realistic fuel chemistry in large-scale computations, *Progress in Energy and Combustion Science* 35 (2009) 192–215.
- [10] S. Vajda, P. Valko, T. Turányi, Principal component analysis of kinetic models, *International Journal of Chemical Kinetics* 17 (1985) 55–81.
- [11] U. Maas, S. B. Pope, Implementation of simplified chemical kinetics based on intrinsic low-dimensional manifolds, *Symposium (International) on Combustion* 24 (1992) 103–112.

- [12] U. Maas, S. B. Pope, Simplifying chemical kinetics: Intrinsic low-dimensional manifolds in composition space, *Combustion and Flame* 88 (1992) 239–264.
- [13] S. H. Lam, D. A. Goussis, The CSP method for simplifying kinetics, *International Journal of Chemical Kinetics* 26 (1994) 461–486.
- [14] S. H. Lam, Using CSP to Understand Complex Chemical Kinetics, *Combustion Science and Technology* 89 (1993) 375–404.
- [15] B. Bhattacharjee, D. A. Schwer, P. I. Barton, W. H. Green, Optimally-reduced kinetic models: Reaction elimination in large-scale kinetic mechanisms, *Combustion and Flame* 135 (2003) 191–208.
- [16] T. Lu, C. K. Law, A directed relation graph method for mechanism reduction, *Proceedings of the Combustion Institute* 30 (2005) 1333–1341.
- [17] T. Lu, C. Law, Strategies for mechanism reduction for large hydrocarbons: N-heptane, *Combustion and Flame* 154 (2008) 153–163.
- [18] P. Pepiotdesjardins, H. Pitsch, An efficient error-propagation-based reduction method for large chemical kinetic mechanisms, *Combustion and Flame* 154 (2008) 67–81.
- [19] K. E. Niemeyer, C.-J. Sung, M. P. Raju, Skeletal mechanism generation for surrogate fuels using directed relation graph with error propagation and sensitivity analysis, *Combustion and Flame* 157 (2010) 1760–1770.

- [20] W. D. Chang, S. B. Karra, S. M. Senkan, A computational study of chlorine inhibition of CO flames, *Combustion and Flame* 69 (1987) 113–122.
- [21] A. Lifshitz, M. Frenklach, Oxidation of cyanogen. ii. the mechanism of the oxidation, *International Journal of Chemical Kinetics* 12 (1980) 159–168.
- [22] A. Fridlyand, M. S. Johnson, S. S. Goldsborough, R. H. West, M. J. McNenly, M. Mehl, W. J. Pitz, The role of correlations in uncertainty quantification of transportation relevant fuel models, *Combustion and Flame* 180 (2017) 239–249.
- [23] F. Harirchi, O. A. Khalil, S. Liu, P. Elvati, A. Violi, A. O. Hero, A data-driven sparse-learning approach to model reduction in chemical reaction networks, *NIPS 2017 Workshop on Advances in Modeling and Learning Interactions from Complex Data*, 2017.
- [24] M. Feinberg, Chemical reaction network structure and the stability of complex isothermal reactors– i. the deficiency zero and deficiency one theorems, *Chemical Engineering Science* 42 (1987) 2229–2268.
- [25] J. Gunawardena, Chemical reaction network theory for in-silico biologists, Notes available for download at <http://vcp.med.harvard.edu/papers/crnt.pdf> (2003).
- [26] D. T. Gillespie, Stochastic simulation of chemical kinetics, *Annu. Rev. Phys. Chem.* 58 (2007) 35–55.

- [27] V. Chellaboina, S. P. Bhat, W. M. Haddad, D. S. Bernstein, Modeling and analysis of mass-action kinetics, *IEEE Control Systems* 29 (2009) 60–78.
- [28] D. F. Anderson, T. G. Kurtz, Continuous time markov chain models for chemical reaction networks, in: *Design and analysis of biomolecular circuits*, Springer, 2011, pp. 3–42.
- [29] U. M. Ascher, L. R. Petzold, *Computer methods for ordinary differential equations and differential-algebraic equations*, volume 61, SIAM, Philadelphia, USA, 1998.
- [30] J. Nocedal, S. J. Wright, *Numerical Optimization*, second ed., Springer, New York, USA, 2006.
- [31] I. Gurobi Optimization, *Gurobi optimizer reference manual*, 2016. URL: <http://www.gurobi.com>.
- [32] I. I. CPLEX, *User’s manual for CPLEX*, Int. Bus. Mach. Corp. 46 (2009) 157.
- [33] Z. Hong, D. F. Davidson, R. K. Hanson, An improved H₂/O₂ mechanism based on recent shock tube/laser absorption measurements, *Combustion and Flame* 158 (2011) 633–644.
- [34] ANSYS, *CHEMKIN version 18.0*, 2016.
- [35] C. K. Law, *Combustion physics*, Cambridge university press, Cambridge, UK, 2010.

- [36] E. L. Petersen, D. M. Kalitan, S. Simmons, G. Bourque, H. J. Curran, J. M. Simmie, Methane/propane oxidation at high pressures: Experimental and detailed chemical kinetic modeling, *Proceedings of the combustion institute* 31 (2007) 447–454.
- [37] S. S. Merchant, C. F. Goldsmith, A. G. Vandeputte, M. P. Burke, S. J. Klippenstein, W. H. Green, Understanding low-temperature first-stage ignition delay: Propane, *Combustion and Flame* 162 (2015) 3658 – 3673.
- [38] H. J. Curran, P. Gaffuri, W. J. Pitz, C. K. Westbrook, A comprehensive modeling study of n-heptane oxidation, *Combustion and flame* 114 (1998) 149–177.
- [39] H. J. Curran, P. Gaffuri, W. J. Pitz, C. K. Westbrook, A comprehensive modeling study of iso-octane oxidation, *Combustion and flame* 129 (2002) 253–280.
- [40] C. Westbrook, W. Pitz, M. Mehl, H. Curran, Detailed chemical kinetic reaction mechanisms for primary reference fuels for diesel cetane number and spark-ignition octane number, *Proceedings of the Combustion Institute* 33 (2011) 185–192.
- [41] S. M. Sarathy, C. K. Westbrook, M. Mehl, W. J. Pitz, C. Togbe, P. Dagaut, H. Wang, M. A. Oehlschlaeger, U. Niemann, K. Seshadri, et al., Comprehensive chemical kinetic modeling of the oxidation of 2-methylalkanes from c7 to c20, *Combustion and flame* 158 (2011) 2338–2357.

- [42] E. Ranzi, A. Frassoldati, R. Grana, A. Cuoci, T. Faravelli, A. Kelley, C. Law, Hierarchical and comparative kinetic modeling of laminar flame speeds of hydrocarbon and oxygenated fuels, *Progress in Energy and Combustion Science* 38 (2012) 468–501.

- [43] Y. Shi, H.-W. Ge, J. Brakora, R. Reitz, Automatic chemistry mechanism reduction of hydrocarbon fuels for hcci engines based on drgep and pca methods with error control, *Energy Fuels* 24 (2010) 1646 – 1654.

Table 3: Influential reactions at selected time samples (see Fig. 1) for H_2/air mixture with the initial condition of 20 atm and 900 K. Influential reactions ($w_{i,k} > 0$) are the same for $\phi = 1$ and $\phi = 2$ except at P5, for which, in fuel-rich conditions, additional 9 reactions are selected.

Condition	Influential Reactions
P1 (all ϕ)	$\text{H} + \text{O}_2 (+\text{M}) \longrightarrow \text{HO}_2 (+\text{M})$ $\text{H} + \text{O}_2 (+\text{O}_2) \longrightarrow \text{HO}_2 (+\text{O}_2)$ $\text{H}_2 + \text{HO}_2 \longrightarrow \text{H} + \text{H}_2\text{O}_2$ $\text{H}_2 + \text{O}_2 \longrightarrow \text{H} + \text{HO}_2$ $\text{H}_2 + \text{OH} \longrightarrow \text{H} + \text{H}_2\text{O}$
P2 (all ϕ)	$\text{H} + \text{O}_2 (+\text{M}) \longrightarrow \text{HO}_2 (+\text{M})$ $\text{H}_2 + \text{HO}_2 \longrightarrow \text{H} + \text{H}_2\text{O}_2$ $\text{H}_2 + \text{OH} \longrightarrow \text{H} + \text{H}_2\text{O}$
P3 (all ϕ)	$\text{H} + \text{O}_2 (+\text{M}) \longrightarrow \text{HO}_2 (+\text{M})$ $\text{H}_2 + \text{OH} \longrightarrow \text{H} + \text{H}_2\text{O}$ $\text{HO}_2 + \text{HO}_2 \longrightarrow \text{O}_2 + \text{H}_2\text{O}_2$
P4 (all ϕ)	$\text{H} + \text{O}_2 (+\text{M}) \longrightarrow \text{HO}_2 (+\text{M})$ $\text{H}_2 + \text{OH} \longrightarrow \text{H} + \text{H}_2\text{O}$ $\text{H}_2\text{O}_2 + \text{H} \longrightarrow \text{H}_2\text{O} + \text{OH}$ $\text{HO}_2 + \text{HO}_2 \longrightarrow \text{O}_2 + \text{H}_2\text{O}_2$
P5 (all ϕ)	$\text{H} + \text{HO}_2 \longrightarrow \text{OH} + \text{OH}$ $\text{H} + \text{HO}_2 \longrightarrow \text{H}_2 + \text{O}_2$ $\text{H} + \text{O}_2 \longrightarrow \text{O} + \text{OH}$ $\text{H}_2 + \text{O} \longrightarrow \text{H} + \text{OH} (\text{DUP})$ $\text{H}_2 + \text{OH} \longrightarrow \text{H} + \text{H}_2\text{O}$ $\text{H}_2\text{O}_2 (+\text{M}) \longrightarrow 2 \text{OH} (+\text{M})$ $\text{H}_2\text{O}_2 + \text{H} \longrightarrow \text{H}_2\text{O} + \text{OH}$ $\text{OH} + \text{HO}_2 \longrightarrow \text{H}_2\text{O} + \text{O}_2$
P5 (only $\phi = 2$)	$2 \text{H} (+\text{M}) \longrightarrow \text{H}_2 (+\text{M})$ $2 \text{H} + \text{H}_2 \longrightarrow 2 \text{H}_2$ $\text{H} + \text{HO}_2 \longrightarrow \text{H}_2\text{O} + \text{O}$ $\text{H} + \text{OH} (+\text{M}) \longrightarrow \text{H}_2\text{O} (+\text{M})$ $\text{H}_2\text{O} + \text{O} \longrightarrow \text{OH} + \text{OH}$ $\text{H}_2\text{O}_2 + \text{H} \longrightarrow \text{HO}_2 + \text{H}_2$ $\text{O} + \text{H} (+\text{M}) \longrightarrow \text{OH} (+\text{M})$ $\text{O} + \text{HO}_2 \longrightarrow \text{OH} + \text{O}_2$ $\text{OH} + \text{H} + \text{H}_2\text{O} \longrightarrow 2 \text{H}_2\text{O}$

Table 4: Low-temperature chemistry subset of the influential reactions at selected times for the combustion of stoichiometric propane/air mixture with the initial condition of 20 atm and 700 K. P1 and P2 correspond to the instances shown in Fig. 3. Species names used in the mechanism [36] are shown. Q stands for olefin, and KET for ketohydroperoxide. Reaction classes are labeled as in [41].

Condition	Influential reactions	Class
P1	$\text{C3H6OOH1-2} \longrightarrow \text{C3H6} + \text{HO2}$	24
	$\text{C3H6OOH2-1} \longrightarrow \text{C3H6} + \text{HO2}$	24
	$\text{C3H6OOH1-3} \longrightarrow \text{C3H6O1-3} + \text{OH}$	25
	$\text{C3H6OOH2-1} + \text{O2} \longrightarrow \text{C3H6OOH2-1O2}$	26
	$\text{C3H6OOH1-3} + \text{O2} \longrightarrow \text{C3H6OOH1-3O2}$	26
	$\text{C3H6OOH1-2} + \text{O2} \longrightarrow \text{C3H6OOH1-2O2}$	26
	$\text{C3H6OOH1-3O2} \longrightarrow \text{C3KET13} + \text{OH}$	27
	$\text{C3H6OOH2-1O2} \longrightarrow \text{C3KET21} + \text{OH}$	27
	$\text{C3H6OOH1-2O2} \longrightarrow \text{C3KET12} + \text{OH}$	27
	$\text{C3KET13} \longrightarrow \text{CH2O} + \text{CH2CHO} + \text{OH}$	28
	$\text{C3KET21} \longrightarrow \text{CH2O} + \text{CH3CO} + \text{OH}$	28
	$\text{C3KET12} \longrightarrow \text{CH3CHO} + \text{HCO} + \text{OH}$	28
	P2	$\text{C3H6OOH2-1} \longrightarrow \text{C3H6} + \text{HO2}$
$\text{C3H6OOH1-2} \longrightarrow \text{C3H6} + \text{HO2}$		24
$\text{C3H6OOH1-3} \longrightarrow \text{C3H6O1-3} + \text{OH}$		25